Molecular Cell, Vol. 19, 449–460, August 19, 2005, Copyright ©2005 by Elsevier Inc. DOI 10.1016/j.molcel.2005.06.034

Structural Basis for the Activation of Microtubule Assembly by the EB1 and p150^{Glued} Complex

Ikuko Hayashi,[1,*] Andrew Wilde,[2] Tapas Kumar Mal,[1] and Mitsuhiko Ikura[1,*]
[1]Division of Molecular and Structural Biology
Ontario Cancer Institute and Department of Medical Biophysics
[2]Department of Medical Genetics and Microbiology
University of Toronto
610 University Avenue
Toronto
Ontario, M5G 2M9
Canada

Summary

Plus-end tracking proteins, such as EB1 and the dynein/dynactin complex, regulate microtubule dynamics. These proteins are thought to stabilize microtubules by forming a plus-end complex at microtubule growing ends with ill-defined mechanisms. Here we report the crystal structure of two plus-end complex components, the carboxy-terminal dimerization domain of EB1 and the microtubule binding (CAP-Gly) domain of the dynactin subunit p150^{Glued}. Each molecule of the EB1 dimer contains two helices forming a conserved four-helix bundle, while also providing p150^{Glued} binding sites in its flexible tail region. Combining crystallography, NMR, and mutational analyses, our studies reveal the critical interacting elements of both EB1 and p150^{Glued}, whose mutation alters microtubule polymerization activity. Moreover, removal of the key flexible tail from EB1 activates microtubule assembly by EB1 alone, suggesting that the flexible tail negatively regulates EB1 activity. We, therefore, propose that EB1 possesses an autoinhibited conformation, which is relieved by p150^{Glued} as an allosteric activator.

Introduction

Microtubules (MTs) play an essential role in cytoskeletal remodeling required for a wide variety of physiological events, such as chromosomal segregation in mitosis and intracellular membrane trafficking in interphase cells. The functions of MTs depend on their dynamic properties, which are highly regulated by a number of proteins including MT-associated proteins (MAPs) and molecular motors (Desai and Mitchison, 1997; Cassimeris, 1999). MTs have an intrinsic structural polarity with fast growing plus-ends directed toward the cell periphery and minus-ends anchored at the centrosome. MT plus-ends display alternating phases of growth and shrinkage, a property of MTs known as dynamic instability (Mitchison and Kirschner, 1984).

A group of proteins called plus-end tracking proteins (+TIPs) associates specifically with MT plus-ends (Howard and Hyman, 2003). +TIPs play a vital role in controlling plus-end dynamics and are responsible for search and capture of MT targets, such as the cell cortex and chromosomes (Schuyler and Pellman, 2001; Carvalho et al., 2003; Mimori-Kiyosue and Tsukita, 2003). The prototype of the plus-end tracking protein is the cytoplasmic linker protein, CLIP-170 (Perez et al., 1999), which contains two CAP-Gly (glycine-rich cytoskeleton associated protein) MT binding domains at its N terminus. CLIP-170 molecules were found to first associate with the MT polymerization ends, then dissociate behind the region of new growth. This treadmilling behavior was observed for other +TIPs, such as EB1 (Mimori-Kiyosue et al., 2000a; Tirnauer et al., 2002a). Recent studies have shown that the yeast CLIP-170 homologs, tip1p and Bik1, form a complex with the kinesin motor proteins, tea2p and Kip2, respectively, and localize to the plus-ends in a kinesin-dependent manner (Busch et al., 2004; Carvalho et al., 2004). Therefore, a more complex mechanism may be involved in targeting of +TIPs to MT plus-ends and their consequent regulation of MT dynamics.

EB1 is a highly conserved member of the +TIP family, initially identified as a binding partner to the tumor suppressor protein, adenomatous polyposis coli (APC) (Su et al., 1995). EB1 localizes at both MT growing ends and the centrosome (Berrueta et al., 1998; Morrison et al., 1998) and has been suggested to play a role in MT dynamics (Tirnauer et al., 1999). APC itself can directly associate with MTs (Munemitsu et al., 1994; Mimori-Kiyosue et al., 2000b) and may also be involved in the control of MT dynamics (Zumbrunn et al., 2001; Barth et al., 2002). The interaction of APC and EB1 enhances MT polymerization in vitro and stabilizes microtubule-kinetocore interactions in vivo (Nakamura et al., 2001; Fodde et al., 2001). In addition to MT and APC binding, EB1 also associates with p150^{Glued}, a component of the dynein/dynactin motor complex (Berrueta et al., 1999; Tirnauer et al., 2002b). A recent report indicates that EB1 and p150^{Glued} may form a ternary complex with MTs to promote MT polymerization, the former via MT elongation and the latter via MT nucleation (Ligon et al., 2003). Evidence of plus-end localization of multiple +TIPs has led to the concept of a MT plus-end complex (Schroer, 2001). However, the organization of the complex is still unclear.

Here, we report the complex structure of two components of the plus-end complex, the carboxy-terminal domain of EB1 (Ec) and the p150^{Glued} CAP-Gly domain (p150N). The heterodimeric contact is located at the hydrophobic cleft of p150N. Using NMR, we defined the EB1 C terminus recognition sites that are not visible in the crystal structure, but crucial for Ec:p150N binding. Interestingly, complete deletion of the p150N binding sites in EB1 results in activation of MT polymerization by EB1 alone. Based on our structural and biochemical

*Correspondence: ihayashi@uhnres.utoronto.ca (I.H.); mikura@uhnres.utoronto.ca (M.I.)

Table 1. Summary of Crystallographic Analysis and Refinement Statistics

Data Collection				
Space group	C2			
Unit cell dimensions	a = 53.1 Å, b = 80.2 Å, c = 39.2 Å, β = 108.5°			
Data Set	**Native**	**SeMet Peak**	**SeMet Edge**	**SeMet Remote**
Wavelength (Å)	0.9513	0.9795	0.9797	0.9643
Data range (Å)	50–1.8	20–2.5	20–2.5	20–2.5
Unique reflections	14,411	10,526	10,591	10,581
Completeness (%)[a]	99.9 (99.5)	98.2 (95.4)	97.9 (94.9)	96.4 (92.2)
I/σ(I)[a]	32.6 (3.8)	15.4 (10.7)	15.5 (10.6)	7.7 (3.6)
R_{merge} [a,b]	0.085 (0.399)	0.048 (0.080)	0.051 (0.087)	0.056 (0.217)
Overall figure of merit	0.63 (SOLVE); 0.91 (DM)			
Refinement				
Resolution range (Å)	25 – 1.8			
No. of reflections in working set	12,545			
R_{cryst} (R_{free})[c]	0.203 (0.243)			
Rmsd bond length (Å)	0.009			
Rmsd bond angles (°)	1.2			
No. of protein atoms	1,096			
No. of solvent atoms	81			
Average B factors (Å^2)				
Protein	32.0			
Ec	30.7			
p150N	32.8			
Ec249-255	42.4			
Water	39.7			
Rmsd B factor for bonded main (side) chain atoms (Å^2)	2.25 (2.69)			

[a] Numbers in parentheses refer to statistics for the highest shell of data (1.90–1.80 Å).
[b] $R_{merge} = \Sigma|I_{obs} - \langle I \rangle|/\Sigma I_{obs}$, where I_{obs} is the intensity measurement and <I> is the mean intensity for multiply recorded reflections (Otwinowski and Minor, 1997).
[c] R_{cryst} and $R_{free} = \Sigma||F_{obs}| - |F_{calc}||/|F_{obs}|$ for reflections in the working and test sets, respectively. The R_{free} value was calculated using a randomly selected 10% of the data set that was omitted through all stages of refinement.

data, we propose a molecular mechanism of EB1-mediated MT assembly.

Results

Overall Structure

Limited tryptic cleavage of EB1 yielded two proteolytically resistant fragments, comprising residues 1–130 and 183–268 (En and Ec, respectively) (Hayashi and Ikura, 2003). Previous biochemical studies showed that each domain is functionally independent: En is responsible for binding to MTs and Ec for binding to APC and $p150^{Glued}$ (Barth et al., 2002; Askham et al., 2002; Bu and Su, 2003). The association of $p150^{Glued}$ with EB1 requires the N-terminal CAP-Gly domain (p150N, residues 16–107), which is also necessary for MT binding of $p150^{Glued}$ (Waterman-Storer et al., 1995). We determined the crystal structure of the Ec:p150N complex using multiple wavelength anomalous diffraction (MAD; Table 1) from a selenomethionine derivative, and refined to 1.8 Å resolution. The Ec:p150N complex forms a heterotetramer of an Ec dimer with two p150N molecules, which is predicted from our chemical cross-linking results (Figure 1A; see the Supplemental Text and Figure S1 with the Supplemental Data available with this article online).

As seen in the recent crystal structure of the EB1 C-terminal domain (Honnappa et al., 2005; Slep et al., 2005), Ec (192–255) forms a coiled-coil domain. It consists of two α helices with a short loop between α1 and α2. α1 of an Ec monomer contains 40 residues presenting a 64 Å long helix that forms a dimer interface with the symmetrically related α1 of the other Ec molecule through the crystallographic screw axis. This structure is identical to the previous Ec structure (PDB code 1WU9; Honnappa et al., 2005; rms deviation for 116 α carbons of 1.0 Å), except for the flexible C-terminal region (248–255) with an extended conformation to provide binding sites for p150N. We could not observe the last 13 residues of Ec (256–268), including the highly acidic tail conserved among EB1 family proteins (Figure 1B).

p150N (25–98) has a β/β structure with three layers of seven β sheets. The structure in complex with Ec is similar to the previous crystal structure of the unbound CAP-Gly domain (Li et al., 2002), except for the β1-β2 loop (rms deviation for 69 α carbons of 0.67 Å). This loop is not involved in Ec binding. In addition, the first nine residues of the p150N structure are disordered. This region forms an α helix with higher temperature factors (B factors) in the unbound form.

Structure of p150N Bound to Ec

In the crystal structure, one p150N molecule buries 9% of the solvent accessible area in the Ec dimer (660 Å^2), which is not as extensive as the Ec homodimer interface (1610 Å^2). The p150N binding region of Ec (249–255) has relatively higher B factors (average 42.4 Å^2,

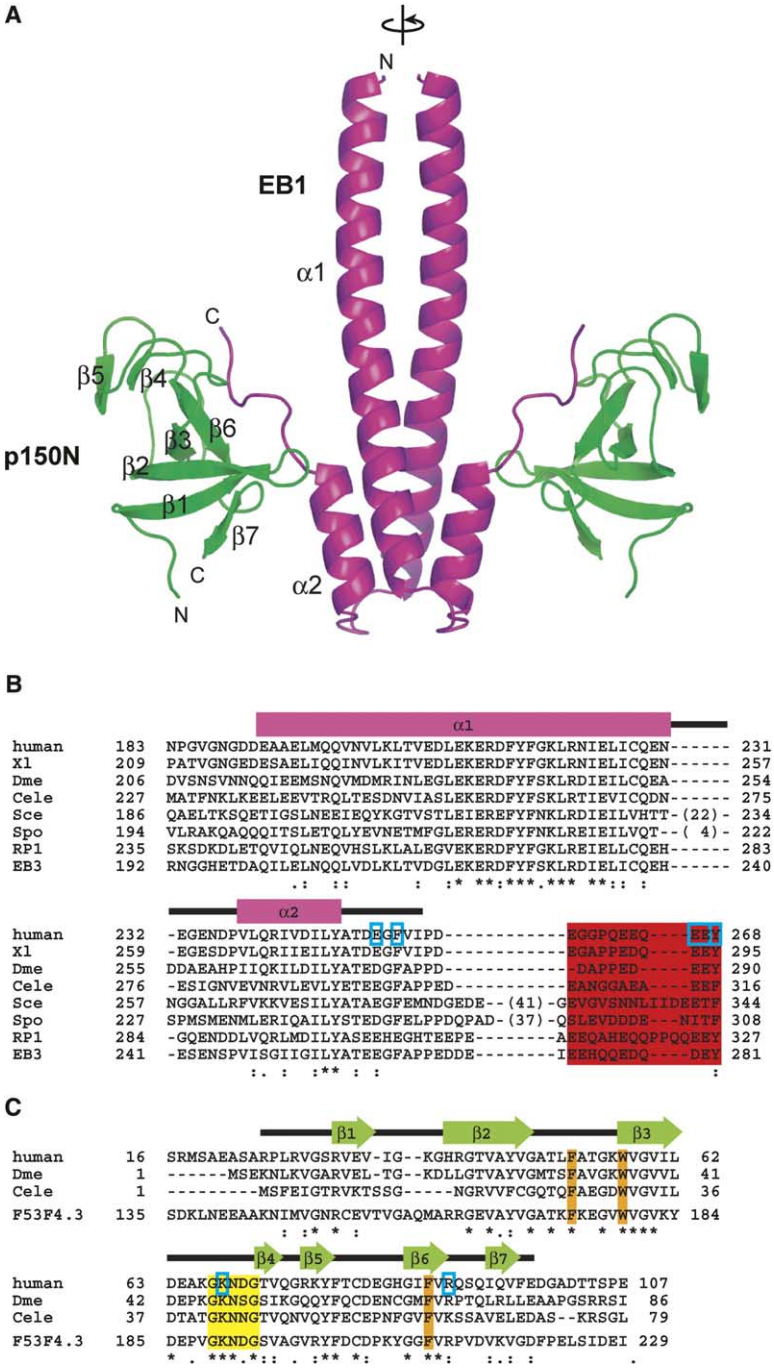

Figure 1. Structure of Ec and p150N Complex

(A) Ribbon representation of Ec (residues 192–255 in magenta) and p150N (residues 25–98 in green), with secondary structure indicated. Molecular 2-fold axis is shown by an arrow. Figures were generated using PyMOL (DeLano, 2001).

(B) Sequence alignment of Ec from six different species and EB1 homologs EB3 and RP1. Homologous sequences are from: human; Xl, *Xenopus laevis*; Dme, *Drosophila melanogaster*; Cele, *Caenorhabditis elegans*; Sce, *Saccharomyces cerevisiae* Bim1; Spo, *Schizosaccharomyces pombe* mal3p; RP1, human RP1; EB3, human EB3. Secondary structural elements are labeled above the sequences. Residues mutated in this study (Glu251, Phe253, Glu266/267, and Tyr268) are boxed in blue. The conserved acidic tail region is highlighted in red.

(C) Sequence alignment of p150N along with another CAP-Gly domain from *C. elegans* F53F4.3 (PDB code 1LPL; Li et al., 2002). The GKNDG motif is shown on a yellow background. Conserved aromatic residues (Phe52, Trp57, and Phe88) in the hydrophobic cleft are shown on orange backgrounds. Lys68 and Arg90 are boxed in blue.

Table1) in comparison with the overall average B factor of Ec (30.7 Å^2), suggesting that the p150N binding region is rather mobile in the Ec structure.

One striking feature of the Ec:p150N complex is the p150N binding region of Ec (Figure 2A). Previous biochemical data showed that a deletion of two amino acids from the C terminus of EB1 completely abolished its binding to p150^{Glued} (Bu and Su, 2003). However, in our crystal structure, p150N binds to the less-conserved loop region flanked by the acidic tail that is completely disordered. The EB1 C-terminal acidic tail has a unique sequence (^{262}QEEQEEY^{268}), which is significantly similar to the α-tubulin C terminus (^{445}EEEGEEY^{451}). This tubulin acidic tail is highly flexible, and could not be observed by cryoelectron crystallography (Nogales et al., 1998). Located on the outer surface of MTs, the tail is predicted to provide an accessible binding site for MAPs. The previous crystallographic study also failed to visualize the C terminus of Ec (Honnappa et al., 2005), suggesting that the flexibility of the acidic tail is a common structural feature between EB1 and tubulin.

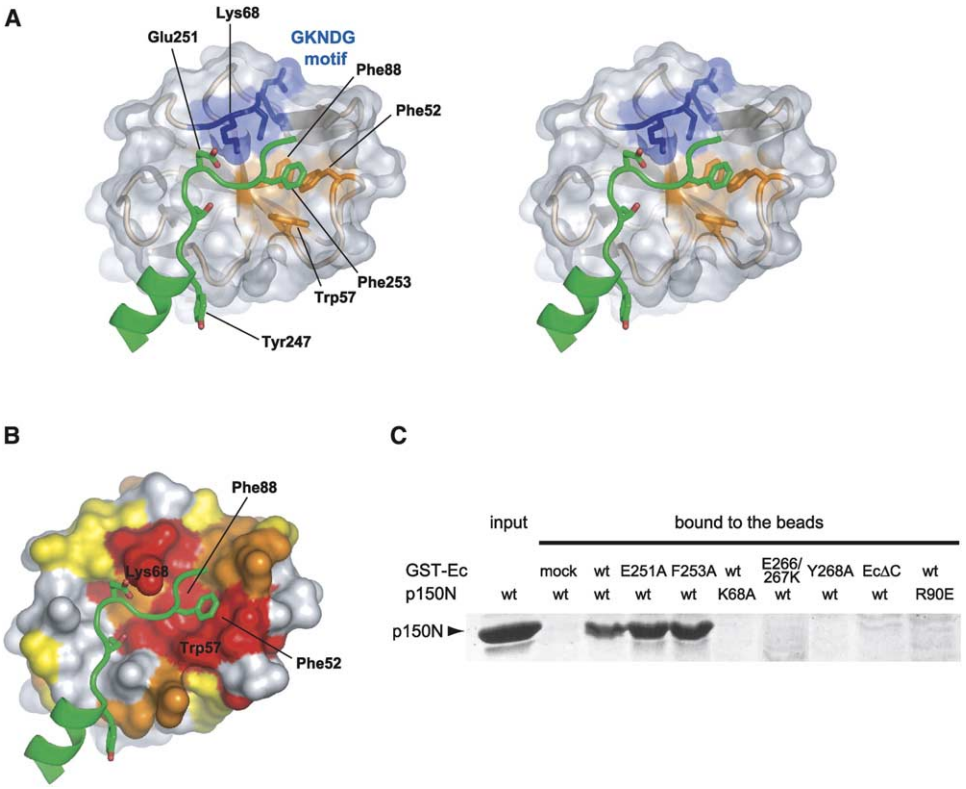

Figure 2. Ec:p150N Interactions

(A) Magnified stereo view focusing on the contact between Ec residues 240–255 and p150N. The α carbons are shown as a cartoon model: Ec is colored green, and p150N beige. The side chain of residues forming protein contacts are shown, with carbon atoms colored according to the backbone; N atoms, blue; O atoms, red. The molecular surface of p150N is shown as transparent. The GKNDG motif is shown in blue, the conserved hydrophobic residues (Phe52, Trp57, and Phe88) in orange.

(B) Sequence conservation mapping of p150N across species: invariant (red), highly conserved (orange), conserved (yellow), and variable (white). The view is in the same orientation as in (A). The invariant aromatic residues (Phe52, Trp57, and Phe88) are labeled along with Lys68 in the GKNDG motif.

(C) In vitro pull-down assay of Ec and p150N, along with their mutants. Binding of p150N, K68A, and R90E was tested for interaction with GST-fused Ec, E251A, F253A, E266/267K, Y268A, and EcΔC. p150N and its mutants were detected by Coomassie-stained SDS-PAGE. Left lane indicates wild-type p150N as a reference. GST-mock is shown as a control.

A previous report (Bu and Su, 2003) showed that residues 208–268 in Ec are required for the formation of a stable complex with p150N. A truncated construct encompassing residues 227–268 retained its ability to bind to p150^{Glued}, but with a reduced affinity. Our structure accounts for these results, whereby the conserved hydrophobic surface of the Ec four-helix bundle (220–247) expands into its tail, providing a greater nonpolar interaction area with p150N (Figures S2A and S2B). The truncated construct distorts the four-helix-bundle formation, leading to destabilization of the whole molecule. In p150N the conserved ^{67}GKNDG^{71} motif, which has been predicted to interact with MTs (Li et al., 2002), is involved in the association with Ec (Figure 2A). The loop containing the GKNDG motif creates a hydrophobic cleft with Phe52 and Trp57 in the β2-β3 loop and Phe88 in the β6 strand. Binding of Ec residues 249–255 buries this highly conserved hydrophobic cleft (Figures 1C and 2B). The invariant residue Lys68 in the GKNDG motif plays a key structural role by engaging in both intra- and intermolecular interactions. The side chain of Lys68 forms a salt bridge with Glu251 and also bonds to the backbone oxygen of Phe253 in Ec, while the backbone nitrogen of Lys68 forms a hydrogen bond with the carbonyl oxygen of Gly86 in β6 of p150N. In order to confirm that Lys68 is critical for the Ec:p150N interaction, we mutated Lys68 to alanine (K68A) and examined Ec binding by in vitro pull-down assay using GST-fused Ec (Figure 2C). K68A abrogates Ec binding, suggesting that Lys68 plays a key role in Ec:p150N complex formation. We also tested two Ec mutants, E251A and F253A, predicted to disrupt the salt bridge with Lys68 in p150N and weaken the hydrophobic interaction with p150N, respectively. Interestingly, both Ec mutants retained binding to p150N. Glu251 is located at the periphery of the hydrophobic pocket with its side chain exposed to the solvent, making no contact with p150N other than the oxygen atom of its carboxyl group, consistent with normal binding. Phe253 is positioned at the center of the hydrophobic cleft, but the mutation did not affect Ec:p150N binding, indicating that the size of the side chain is not critical at this position.

Probing p150N-EB1 Tail Interactions

Previous biochemical studies (Bu and Su, 2003) suggested that the C-terminal tail of Ec, especially the last two residues (Glu267 and Tyr268), is essential for the

association of EB1 with p150^{Glued}. We constructed three Ec mutants, one corresponding to the observed Ec crystal structure, EcΔC (183–256; summarized in Figure 5B), and the other with mutations in the acidic tail, Glu266 and Glu267 to Lys (E266/267K) and Tyr268 to Ala (Y268A), and examined their binding ability to p150N by pull-down assay (Figure 2C). All three mutants showed a complete loss of affinity to p150N, emphasizing that both acidic and aromatic residues are required in Ec:p150N complex formation.

In order to gain further insight into the interaction between the Ec C-terminal tail and p150N, we employed NMR spectroscopy. Excellent peak dispersion was observed in a ^{1}H-^{15}N HSQC spectrum of uniformly ^{15}N-labeled p150N (Figure S3A). We first examined the titration of the EB1 tail peptide (247–268) to ^{15}N-labeled p150N (Figure S3B). The observed chemical shift perturbation in the HSQC spectrum revealed the EB1 tail interaction sites that were not observed in the crystal structure (see below). However, this strategy failed to observe the resonances from the EB1 acidic tail, since the EB1 peptide was not labeled with ^{15}N. To assist mapping of thus far invisible EB1 tail interaction sites with p150N, we generated a chimera of p150N with the EB1 tail at its C terminus (hereafter named p150N:EB1$_{tail}$). The HSQC spectrum of ^{15}N-labeled p150N with the unlabeled EB1 peptide was essentially identical to that of ^{15}N-p150N:EB1$_{tail}$ (Figure 3A), indicating that this chimeric construct retains the native interaction between Ec and p150N, hence providing a model system to probe the Ec:p150N interaction by NMR spectroscopy. With the uniformly labeled p150N:EB1$_{tail}$ sample, we could not sequentially assign the last 13 residues due to the absence of an NH atom at Pro261 and severely overlapping peaks from glutamate residues at 263–267. However, by introducing the tyrosine-specific labeling, we were able to identify the last Tyr268 (Figure S5B). The resonance of Tyr268, found at 8.45 ppm, (^{1}H) and 127.6 ppm (^{15}N) in wild-type p150N:EB1$_{tail}$, was markedly shifted to 8.05 ppm and 126.9 ppm, respectively, when the K68A mutation was introduced. The observed chemical shift change for Tyr268 was also accompanied by drastic changes in mobility as evidenced by ^{15}N-{^{1}H} NOE measurements (see below).

The chemical shift changes observed for p150N upon addition of the EB1 tail peptide can be attributed to p150N's binding interface with the EB1 C-terminal tail. These changes are also observed in the NMR spectrum of the chimera p150N:EB1$_{tail}$. All of these perturbed residues within p150N are mapped on the crystal structure of p150N (Figure 3B), which are mainly found in the vicinity of the hydrophobic cleft. In addition to this hydrophobic cleft, two other segments were perturbed: Ala49 to Leu51 and Ser91 to Gln95. The former segment is located in the β2-β3 loop at the periphery of the hydrophobic cleft in p150N and the latter in β7, but both do not participate in the direct interaction with Ec in the crystal structure. Therefore, we conclude that residues 49–51 and 91–95 are involved in the crystallographically invisible EB1 tail interactions.

Previous biochemical analysis (Bu and Su, 2003) and our in vitro experiments showed that Tyr268 in EB1 tail is essential for Ec:p150N binding (Figure 2C and Figure S3C). However, we were unable to observe Ec tail in the crystal structure. We believe that this interface resulted from nonphysiological crystal packing interactions in high salt (1.75 M ammonium sulfate), disrupting the ionic interaction of the Ec acidic tail with p150N (Figure S4).

We modeled the C-terminal tail of EB1 into the Ec:p150N structure by tracing the residues which experienced spectral perturbations of the EB1 tail as described above (Figure 3B). An excellent fit of the EB1 C-terminal tail is achieved, in which the Tyr268 side chain fits into the groove of Ile94 and Gln95, two residues that undergo drastic chemical shift changes. In addition, the carboxyl group of Glu266 in EB1 acidic tail forms a salt bridge to the guanidinium group of Arg90 in p150N. In order to validate this model, we made single and double mutants of p150N:EB1$_{tail}$, Arg90 in p150N to Glu (R90E) and two Glu residues at 266 and 267 in EB1 tail to Lys (E266/267K). These p150N:EB1$_{tail}$ mutants failed to form intramolecular interactions between p150N and EB1 tail, as judged by the HSQC experiments (data not shown). We labeled four tyrosine residues in these chimeric proteins with ^{15}N (Tyr 46 and 78 in p150N and 247 and 268 in EB1 tail; Figure S5AB) and measured backbone ^{15}N-{^{1}H} NOEs to probe backbone mobility (Figure 3C). The positive NOE value observed for Tyr268 in wild-type p150N:EB1$_{tail}$ is drastically reduced by either mutation of Lys68, Glu266/267, or Arg90, indicating an increased mobility of these residues. These results are consistent with the loss of affinity in the in vitro pull-down assay (Figure 2C). In contrast, the rest of three tyrosine residues, Tyr46, Tyr78, and Tyr247, that do not participate in p150N:EB1$_{tail}$ interactions, show few changes in their backbone mobility by mutations. Again, the NOE experiment is in agreement with our in vitro experiments, which show that Tyr268 is a recognition determinant of EB1:p150N complex formation.

Roles of Interactions between EB1 and the CAP-Gly Domain of p150^{Glued}

It has been suggested that EB1 and p150^{Glued} have different effects on MT polymerization in vitro: p150^{Glued} on MT nucleation effect and EB1 on MT elongation (Ligon et al., 2003). To examine the functional roles of EB1 and the CAP-Gly domain of p150^{Glued} on tubulin polymerization, we performed light scattering assays using our EB1 and p150N constructs. Since tubulin polymerizes more efficiently in the presence of nucleating MT seeds, experiments were performed in the presence or absence of seeds. In the absence of seeds, only the EB1:p150N complex could produce an increase in the optical turbidity of tubulin solution (Figure 4A). This MT assembly activity was completely abolished when p150N was replaced with mutants K68A or R90E. Similarly, the EB1 mutant lacking the acidic tail (EB1ΔC, 1–256) failed to promote MT polymerization. These results are consistent with our microscope observation (Figure 4C): the combination of the wild-types produced dense MT bundles, whereas the introduction of mutations in either protein generate only short MTs and some thin bundles. The addition of seeds to tubulin solution allowed MT assembly with these malfunctional mutant combinations (Figure 4B). K68A with EB1 recovered half the activity of wild-type EB1:p150N, which is consistent with the NMR result that K68A weakly in-

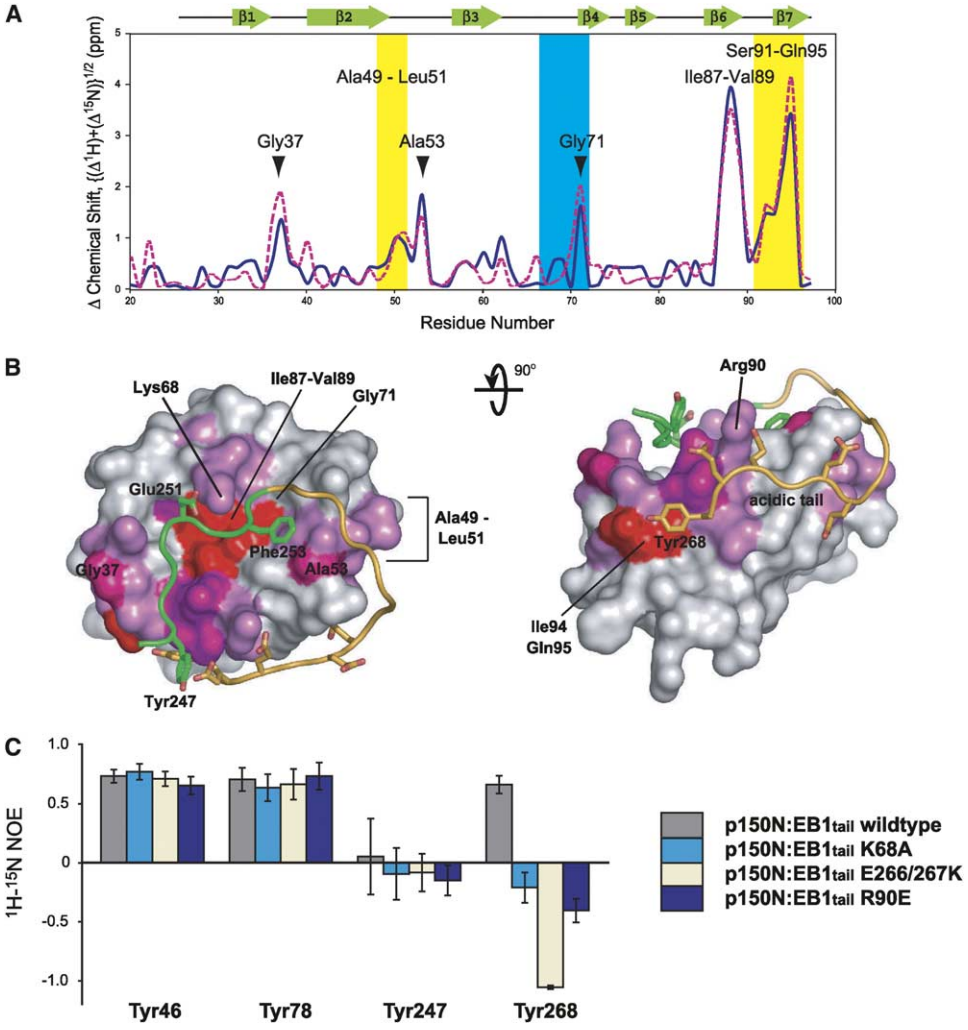

Figure 3. Binding of EB1 Tail to p150N

(A) Measured chemical shift changes versus residue number for p150N upon binding of the EB1 tail of p150N:EB1$_{tail}$ (blue solid line) or the peptide (magenta dot), represented as $(\Delta H^2 + \Delta N^2)^{1/2}$ in ppm. For peptide binding, the chemical shifts of ^{15}N-p150N with three molar equivalents of the peptide are used for plotting. Residues with large chemical shift perturbations are labeled. The GKNDG motif region is highlighted in blue. The EB1 acidic tail interaction sites predicted in this study are shown on a yellow background. The locations of p150N structural elements are shown on top.

(B) Chemical shift perturbations in p150N due to binding of the EB1 tail, mapped onto the molecular surface of p150N. The EB1 tail observed in the crystal structure is shown in green. Color ramp from white to red indicates a 0 to 4 ppm change. The left-hand view is in the same orientation as Figure 2A. The view on the right is rotated 90° around the x axis. Hypothetical model of the EB1 C-terminal tail (residues 256–268) is docked onto p150N and shown in yellow. The side chains of the glutamate residues in the Ec acidic tail (Glu263, 264, 266, and 267) are shown as sticks.

Largest chemical shift changes are observed for the residues from Ile87 to Val89 in the hydrophobic cleft and the surrounding residues of Gly37, Ala53, and Gly71. The chemical shift change in Ala53 (~2 ppm) was induced by the ring-current effect of Phe253, supporting hydrophobic interactions between p150N and the EB1 tail. The residues discussed in the text are labeled.

(C) ^{15}N-{^{1}H} NOE measurements of four tyrosine residues (46 and 78 in p150N, 247 and 268 in EB1 tail; Figure S5A) in p150N:EB1$_{tail}$ and its mutants, K68A, E266/267K, and R90E.

teracts with EB1 tail (Figure S3C). R90E with EB1 showed one-third of wild-types' turbidity and similar kinetics to EB1ΔC with p150N, supporting our model that Arg90 is one of the recognition sites of EB1 tail. These mutant combinations produced MT bundles, but their tangles are smaller than those of the wild-types (Figure 4D). When we replaced EB1 with a pair of EB1 half fragments, En and Ec, no increase in turbidity was observed regardless of MT seeds. These results indicate that p150N binding to intact EB1 is essential for the synergy of EB1 and p150N to stimulate MT assembly.

Our data showed that p150N alone did not stimulate MT polymerization without seeds (Figure 4A and Figure S6), indicating that p150N does not effect MT nucleation. This result is in disagreement with the previous observation on MT polymerization stimulated by p150^{Glued} (1–300) (Ligon et al., 2003). This is presumably due to p150N's lack of a conserved basic serine-rich region

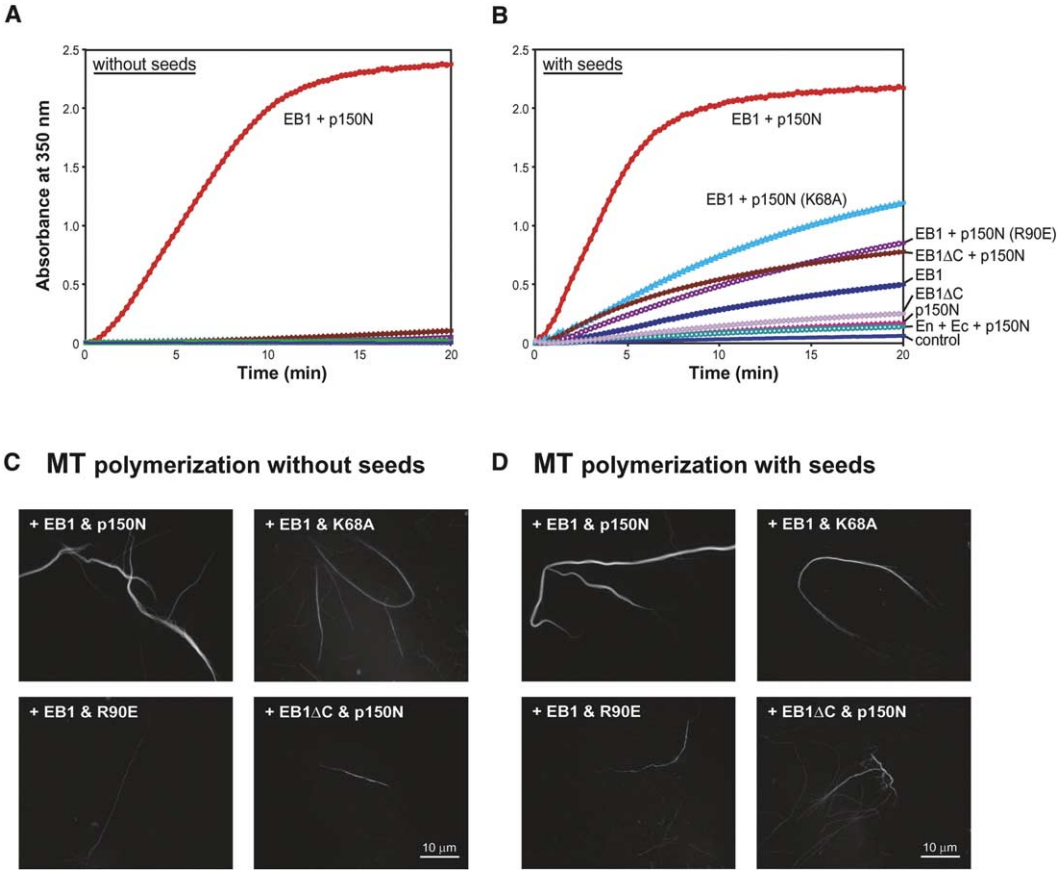

Figure 4. Association of EB1 and p150N Is Important in Promoting Tubulin Polymerization

(A) The kinetics of tubulin polymerization as measured by the increase in sample absorption at 350 nm in the absence of seeds. The combination of both wild-type EB1 and p150N had a greater effect (red), whereas the combinations with mutants (pair of En and Ec, EB1ΔC for EB1 and K68A, R90E for p150N) did not increase the turbidity.

(B) The kinetics of tubulin polymerization in the presence of seeds. In both (A) and (B), En, Ec, and p150N mutants K68A and R90E did not show any turbidity by themselves (data not shown).

(C and D) Fluorescently labeled MTs induced by EB1 and p150N or their mutants in the absence (C) or presence (D) of seeds. The reaction mixtures at 10 min were transferred onto the coverslips and visualized. Scale bar, 10 μm. MTs induced by EB1 or p150N alone are shown in Figure S6.

(111–191) required for efficient binding to MTs (Hoogenraad et al., 2000), which is adjacent to the p150N (25–98). The weak affinity of p150N to MTs may explain the deficiency of MT polymerization by p150N alone, and may also result in the effective synergy of EB1 and p150N in the presence of seeds. With the construct of p150Glued (1–330), EB1 may compete with the serine-rich region upon MT binding, resulting in MT polymerization inefficiency.

EB1 Alone Can Promote MT Assembly In Vitro

MT assembly analysis suggests that EB1 tail has a functional role in MT polymerization. Our crystal structure indicates that Ec binds to the putative MT binding sites of p150N (Li et al., 2002), raising the possibility that p150N forms a complex with Ec, but not with MTs, during the MT assembly reaction. To examine whether p150N binds Ec and MTs on the same binding sites, MT binding abilities of p150N mutants K68A and R90E were analyzed by cosedimentation assay (Figure 5A). Both mutations drastically decreased p150N's affinity for MTs in a similar manner observed for Ec, indicating that the MT binding sites coincide with the Ec binding sites in p150N. In order to investigate whether p150N can bind MTs and Ec simultaneously, we performed a competitive binding assay of p150N against MTs with Ec or its mutant EcΔC as an antagonist (Figure 5C). Preincubation of p150N with Ec abolished MT binding by p150N, due to the complex formation between p150N and Ec. This result is consistent with the previous in vivo observation that the overexpression of C-terminal EB1 causes a reduction of MT plus-end-associated p150Glued (Bu and Su, 2003). On the other hand, EcΔC did not affect MT binding by p150N, demonstrating the significance of Ec tail in the Ec:p150N complex.

To elucidate the functional role of the Ec:p150N interaction, we evaluated the effect of Ec on MT polymerization with the EB1:p150N complex (Figure 5D). The

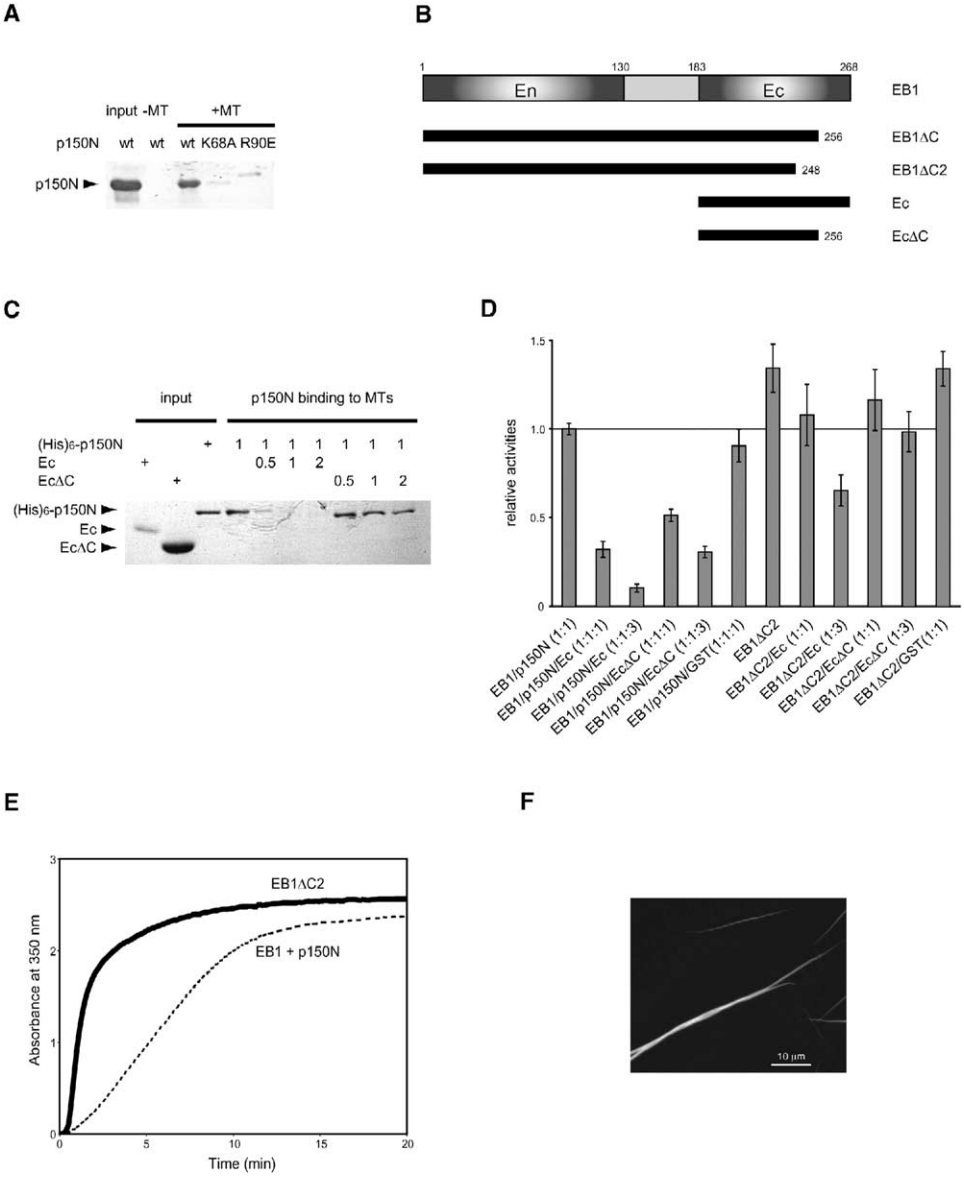

Figure 5. EB1 Is a Regulator of MT Assembly

(A) In vitro MT binding of p150N and its mutants. p150N and its mutants, K68A and R90E, were cosedimented with MTs. MT binding is demonstrated by the appearance of p150N in the pellet. Both mutants abolish MT binding.

(B) Schematic of EB1 deletion mutants used in this study.

(C) Competition between MTs and Ec or EcΔC for p150N binding. 3.5 pmol p150N and increasing amounts (0.5, 1, and 2 equimolar amounts) of Ec or EcΔC were preincubated with p150N and applied to the MT binding analysis. Cosedimented p150N with MTs is shown by an arrow. Addition of excess amounts of Ec inhibits the interaction between p150N and MTs, whereas EcΔC does not affect p150N binding to MTs.

(D) Effect of Ec or EcΔC in MT assembly with EB1:p150N or EB1ΔC2. After an incubation of the EB1:p150N complex, one or three equimolar amounts of Ec were added to the solution and their MT assembly was examined. Relative activity of each reaction was compared by tubulin turbidity at 350 nm after 10 min incubation at 37°C. GST was used as a negative control, showing no significant inhibition of the activity. Turbidity increased by the EB1:p150N complex alone was used as a reference. Error bar, SD for the mean values of three experiments carried out in duplicate.

(E) EB1ΔC2 promotes MT polymerization without p150N. EB1ΔC2 (solid line) can induce MT assembly with faster kinetics than the EB1:p150N complex (dotted line).

(F) MT bundle formation by the addition of EB1ΔC2 in tubulin solution. The reaction mixture at 10 min was transferred onto the coverslip and visualized. Scale bar, 10 μm.

addition of Ec to EB1:p150N drastically decreased the turbidity of tubulin solution, suggesting that Ec inhibited the activation by EB1:p150N. When EcΔC was mixed to EB1:p150N in a 1:1 molar ratio, EcΔC also displayed a reduced inhibitory effect on MT polymerization (~50% of the original activity), which was not detected by the aforementioned in vitro binding analysis. These results indicate that the inhibition of p150N binding to EB1 causes a defect in MT assembly.

Surprisingly, an EB1 fragment lacking the whole

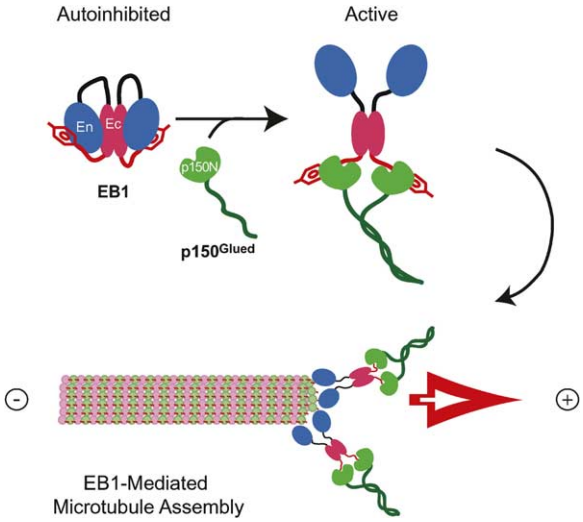

Figure 6. A Model of EB1-Mediated MT Assembly

A hypothetical model of EB1-dependent MT assembly. In the absence of p150Glued, we propose that EB1 C-terminal domain (Ec) binds the N terminus (En) and masks the MT binding sites. Binding to the p150Glued dimer via the EB1 tail releases En from the repressed state and activates MT assembly in an EB1-dependent manner. The distance between the N terminus of Ec and the p150N binding site, which is overlapped with the putative APC binding site (Honnappa et al., 2005), is ~45 Å; the diameter of the globular domain En is ~30 Å; the flexible intermediate domain between En and Ec is ~60 residues (180–210 Å). Taken together, the autoinhibited model of EB1 would be feasible, consistent with our in vitro analyses. Note that we illustrate a model in which an EB1 dimer binds to a p150Glued dimer. However, it is feasible that two p150N domains interact with multiple EB1 molecules to form a multimeric complex, since p150N is connected by a long predicted linker (110 residues) to form a dimer (Gill et al., 1991).

p150N binding region (EB1ΔC2, 1–248) showed an enhanced activity with faster kinetics than EB1:p150N (Figures 5D–5F). This observation suggests that EB1 has an intrinsic ability to promote MT assembly, but the flexible tail (249–268) internally inhibits the activity. Such interference raises the possibility that the EB1 MT binding domain (En) is autoinhibited by the flexible tail (Figure 6). To test this hypothesis, we measured the MT polymerization activity of EB1ΔC2 in the presence of Ec or EcΔC (Figure 5D), which revealed a 20% and 15% decrease in the 1:1 mixture of EB1ΔC2 with Ec and EcΔC, respectively. Further, we measured ^{1}H-^{15}N HSQC spectra of uniformly ^{15}N-labeled En to examine the interaction between En and Ec (Figure S7). The excellent chemical shift dispersion observed with ^{15}N-labeled En was largely suppressed by the addition of unlabeled Ec. The NMR data strongly suggest the existence of the interaction between En and Ec, consistent with the negative regulation of the flexible tail on EB1 activity.

Discussion

Structural Property of EB1 MT Binding Domain

A subset of MAPs localizes at the plus-ends of growing MTs (Perez et al., 1999; Berrueta et al., 1998; Mimori-Kiyosue et al., 2000b; Vaughan et al., 2002). Each of these proteins possesses a MT binding domain, and a common structural feature of these domains is a hydrophobic patch rather than the basic surface commonly found in many other MT binding proteins (Li et al., 2002; Hayashi and Ikura, 2003). EB1 and p150Glued both bind to MTs but possess different types of MT binding domain. EB1 MT binding domain (En) reveals a calponin homology (CH) domain fold of six α helices, whereas p150Glued CAP-Gly domain has a β/β structure, implying that they associate with MTs in different manners to exert functionally distinct effects.

The CH domain has been found as a tandem pair in many actin binding proteins, such as fimbrin and utrophin (Gimona et al., 2002). Biochemical and crystallographic studies revealed that a pair of CH domains utilizes the hydrophobic patches to target actin (Goldsmith et al., 1997; Keep et al., 1999). One of the exceptions is IQGAP, which contains a single CH domain in its sequence. The CH domain of IQGAP can interact with actin (Mateer et al., 2004) but cannot target itself to actomyosin through actin without its C-terminal coiled-coil dimerization domain (Lippincott and Li, 1998). This indicates that the dimerization domain functions as a mediator that positions two CH domains in the orientation required for function. In EB1, Ec is a dimerization domain (Honnappa et al., 2005; this study), suggesting that EB1 functions in a manner similar to IQGAP. Indeed, MT elongation is efficiently achieved by EB1 dimerization, as the En monomer can bind but cannot stabilize MTs (Bu and Su, 2003; this study). It is also tempting to speculate that the CH domain is designed to bind both actin and microtubule cytoskeletal filaments through its hydrophobic surface property.

Implications for Mechanism of EB1-Mediated MT Assembly

Our data show that the activation of MT polymerization requires the C terminus of EB1 (Ec), illuminating the key role of Ec in EB1-mediated MT assembly. We propose the existence of an Ec-imposed latent conformation of EB1 (Figure 6). As shown previously, En and Ec are connected with a flexible intermediate domain (134–192) (Honnappa et al., 2005). The length of this flexible domain can be 180–210 Å, in theory, which enables one to speculate that EB1 has a head-to-tail association. The dynactin subunit p150Glued is a dimeric protein whose N-terminal CAP-Gly domain (p150N) is flanked by ~110 aa of predicted loop (Gill et al., 1991). The EB1 flexible intermediate domain and the predicted loop region in p150Glued may be critical for the interaction between EB1 and the dynactin complex to form an extended multimeric complex of these two components. Although physiologically relevant stoichiometry between an EB1 dimer and the dynactin complex is unknown, the p150Glued dimerization may allow a dynactin complex to effectively associate with an EB1 dimer or multiple EB1 molecules. Binding of p150Glued relieves the autoinhibitory contact within EB1, leading to an activation of EB1-mediated MT assembly. The effect of p150Glued resembles that of the signal transduction proteins functioning as modular allosteric switches (Lim, 2002). Notably, the plus-end tracking protein, CLIP-170, has a similar autoinhibitory mechanism in a head-to-tail fashion that is relieved by p150Glued (Lansbergen et al.,

2004). EB1 may extend this theme to cytoskeletal structural proteins to control MT dynamics. It should be noted that the En:Ec interaction is fairly weak, since their association is not observed in size exclusion column chromatography (data not shown) and is in an intermediate exchange regime shown on the NMR timescale, which typically corresponds to K_d of 10^{-3}–10^{-5} M. In a previous structural study of Ec, the electron microscopy analysis of EB1 did not show the interaction between En and Ec (Honnappa et al., 2005), presumably because of the high concentration of glycerol in the protein solution (30%), which inhibited the intramolecular interaction. Further structural analyses are needed to elucidate the EB1 autoinhibitory mechanism.

EB1 also binds APC (Su et al., 1995). Given that APC can promote MT polymerization with EB1 in vitro (Nakamura et al., 2001), it is possible that APC also induces EB1 conformational changes into an unfurled active form. This idea is supported by the report of Ec crystal structure that the putative APC binding sites are located close to the p150N binding sites (Honnappa et al., 2005) and that they bind exclusively to EB1 (Askham et al., 2002). Recently, a ternary complex of EB1, APC, and mDia was shown to stabilize MTs in fibroblasts (Wen et al., 2004). APC may interact with EB1 in a similar manner to $p150^{Glued}$ to stimulate MT assembly and to provide mDia binding sites within the N-terminal domain of EB1.

The present study has raised a new hypothesis that EB1 is a regulator of MT dynamics and that other components, such as $p150^{Glued}$ and APC, may act as contributors to EB1, subsequently forming a plus-end complex at MT growing ends. We note that yeast EB1 homolog mal3p is involved in recruiting the CLIP-170 homolog tip1p to MT plus-ends (Busch and Brunner, 2004). A future direction will be to elucidate how plus-end remodeling is achieved by multiple +TIPs, in order to regulate MT dynamics during mitosis.

Experimental Procedures

Protein Expression and Purification

The C-terminal dimerization domain of human EB1 (Ec, residues 183–268) was identified by trypsinization of full-length EB1 as previously described (Hayashi and Ikura, 2003). The cDNA sequences of EB1 and Ec were amplified by PCR and cloned into pGEX4T-1 (GE Healthcare). Proteins were expressed in *E. coli* strain BL21(DE3). GST fusion proteins were purified with a GSTrap column (GE Healthcare). The GST tag was cleaved with thrombin (Sigma) and removed by further purification with HiTrapQ (GE Healthcare). The selenomethionine-substituted Ec fragment was expressed in BL21(DE3) as described (Hayashi and Ikura, 2003) and purified as for the wild-type protein.

The cDNA fragment of the CAP-Gly domain in $p150^{Glued}$ (p150N, residues 16–107) was generated by PCR from human brain cDNA libraries and inserted into pET15b (Novagen). The protein was expressed with BL21(DE3) and purified with HiTrap chelating column (GE Healthcare). After cleavage of the His tag by thrombin, the protein was loaded onto HiTrapSP. Ec and p150N were separately concentrated to 25 mg/ml in 10 mM Tris (pH 7.5), 0.1 M NaCl, and 1 mM DTT, and mixed to 1:1 for crystallization.

Amino acid mutations were introduced using the QuickChange Site-Directed Mutagenesis Kit (Stratagene). For all the constructs, the absence of error was confirmed by DNA sequencing.

Crystallography

Crystals of the Ec and p150N complex were obtained by the sitting drop vapor diffusion method at room temperature. Two microliters of protein solution were mixed with an equal volume of well solution with 0.1 M MES (pH 6.5) and 1.75 M ammonium sulfate. Each fragment was intact as confirmed by mass spectroscopy. Crystals belong to space group C2 with cell dimensions a = 53.1 Å, b = 80.2 Å, c = 39.2 Å, β = 108.5°. The asymmetric unit contains two molecules of each fragment and a solvent content of 55%. For data collection, crystals were transferred into cryoprotectant solutions containing 27% glycerol in mother liquor and flash frozen in liquid nitrogen. All data sets were collected at the Advanced Photon Source (Argonne, IL) on beamline 19-BM. Data processing and reduction were carried out with the HKL2000 program suit (Otwinowski and Minor, 1997). Position of one selenium atom in Ec was found using SOLVE (Terwilliger and Berendzen, 1999). Phases were improved and extended to 1.8 Å with DM (CCP4, 1994). The initial model was built with ARP/wARP (Perrakis et al., 1999). Manual rebuilding was performed with XtalView (McRee, 1999), followed by iterative rounds of refinement using simulated annealing and positional refinement in CNS (Brunger et al., 1998).

Design of the p150N-EB1 Tail Chimera

The construct of the chimeric protein with $p150^{Glued}$(16–107) and EB1(247–268) was designed based on the Ec:p150N crystal structure. The cDNA sequences of $p150^{Glued}$(16–107) and EB1(247–268) were amplified by PCR using primers that contain a $(Gly)_3$ linker sequence in frame. Two fragments were combined by a second PCR reaction. The resulting cDNA fragment, which codes $p150^{Glued}$(16–107)-$(Gly)_3$-EB1(247–268), was cloned in pET15b. The His-tag fused chimeric protein p150N:$EB1_{tail}$ was expressed and purified in the same manner as for p150N. p150N:$EB1_{tail}$ eluted as a monomer in the size exclusion column and did not promote tubulin polymerization with EB1 (data not shown), indicating that p150N interacts with EB1 tail in an intramolecular manner.

NMR Spectroscopy

All NMR experiments were recorded at 298K on Varian INOVA 500 and 600 MHz spectrometers equipped with a triple resonance pulse field gradient. Protein samples prepared for the structural analyses contained 2 mM uniformly ^{15}N- or $^{15}N/^{13}C$-labeled p150N or p150N:$EB1_{tail}$ in 10 mM Bis-Tris (pH 6.5), 100 mM NaCl, 1 mM DTT, and 10% D_2O. Data were processed with nmrPipe (Delaglio et al., 1995), and analyzed using Xeasy (Bartels et al., 1995). Resonance assignment for the backbone of both peptides was accomplished using HNCACB and CBCA(CO)NH (Sattler et al., 1999). The ^{15}N-{^1H} NOEs were measured using ^{15}N-Tyr-labeled proteins (see Supplemental Experimental Procedures) by comparison of spectra recorded with or without ^1H saturation.

Tubulin Polymerization Assay and MT Pelleting

Tubulin was isolated from bovine brain and labeled with rhodamine (Rh-tubulin) as described (Hyman et al., 1991). MT seeds were prepared as described by Ligon et al. (2003). Tubulin polymerization was measured in a light scattering assay (Schiff et al., 1979). The turbidity was recorded as the optical absorbance at 350 nm using a Varian CARY 300Bio UV-VIS spectrophotometer in 15 s intervals at 37°C. The reaction was initiated by adding 10 μl of a 20 mg/ml purified tubulin solution to 110 μl of a buffer containing 10 μM of EB1 and/or p150N and their derivatives in PMEM (50 mM K-PIPES, 50 mM MES, 1 mM EGTA, 1 mM $MgCl_2$, 1 mM GTP [pH 6.8]), in the presence or absence of 10 μg MT seeds. For microscopic analyses, ~15% Rh-tubulin was added to unlabeled tubulin. After 10 min of reactions, MTs were fixed in 1% glutaraldehyde, pelleted onto coverslips (Mitchison and Kirschner, 1984), and viewed on a Nikon E800 epifluorescent microscope. Images were captured using an Orca-ER CCD camera (Hamamatsu) with MetaMorph software (Universal Imaging). MT cosedimentation assay was described previously (Hayashi and Ikura, 2003).

Supplemental Data

Supplemental Data are available with this article online at http://www.molecule.org/cgi/content/full/19/4/449/DC1/.

Acknowledgments

We thank Avijit Chakrabartty for the assistance with AUC analysis, Ahmad Khorchid and Jane Gooding for critical reading of the manuscript, and the staff of the Advanced Photon Source for assistance with the data collection. This work was supported by the grants from National Cancer Institute of Canada (NCIC). I.H. acknowledges the Canadian Institutes of Health Research (CIHR) for a postdoctoral fellowship. M.I. holds a Canada Research Chair in Cancer Structural Biology.

Received: March 9, 2005
Revised: May 19, 2005
Accepted: June 29, 2005
Published: August 18, 2005

References

Askham, J.M., Vaugham, K.T., Goodson, H.V., and Morrison, E.E. (2002). Evidence that an interaction between EB1 and p150(Glued) is required for the formation and maintenance of a radial microtubule array anchored at the centrosome. Mol. Biol. Cell *13*, 3627–3645.

Bartels, Ch., Xia, T.-H., Billeter, M., Güntert, P., and Wüthrich, K. (1995). The program XEASY for computer-supported NMR spectral analysis of biological macromolecules. J. Biomol. NMR *5*, 1–10.

Barth, A.I., Siemers, K.A., and Nelson, W.J. (2002). Dissecting interactions between EB1, microtubules and APC in cortical clusters at the plasma membrane. J. Cell Sci. *115*, 1583–1590.

Berrueta, L., Kraeft, S.K., Tirnauer, J.S., Schuyler, S.C., Chen, L.B., Hill, D.E., Pellman, D., and Bierer, B.E. (1998). The adenomatous polyposis coli-binding protein EB1 is associated with cytoplasmic and spindle microtubules. Proc. Natl. Acad. Sci. USA *95*, 10596–10601.

Berrueta, L., Tirnauer, J.S., Schuyler, S.C., Pellman, D., and Bierer, B.E. (1999). The APC-associated protein EB1 associates with components of the dynactin complex and cytoplasmic dynein intermediate chain. Curr. Biol. *9*, 425–428.

Brunger, A.T., Adams, P.D., Clore, G.M., DeLano, W.L., Gros, P., Grosse-Kunstleve, R.W., Jiang, J.S., Kuszewski, J., Nilges, M., Pannu, N.S., et al. (1998). Crystallography & NMR system: a new software suite for macromolecular structure determination. Acta Crystallogr. D *54*, 905–921.

Bu, W., and Su, L.K. (2003). Characterization of functional domains of human EB1 family proteins. J. Biol. Chem. *278*, 49721–49731.

Busch, K.E., and Brunner, D. (2004). The microtubule plus end-tracking proteins mal3p and tip1p cooperate for cell-end targeting of interphase microtubules. Curr. Biol. *14*, 548–559.

Busch, K.E., Hayles, J., Nurse, P., and Brunner, D. (2004). Tea2p kinesin is involved in spatial microtubule organization by transporting tip1p on microtubules. Dev. Cell *6*, 831–843.

Carvalho, P., Tirnauer, J.S., and Pellman, D. (2003). Surfing on microtubule ends. Trends Cell Biol. *13*, 229–237.

Carvalho, P., Gupta, M.L., Jr., Hoyt, M.A., and Pellman, D. (2004). Cell cycle control of kinesin-mediated transport of Bik1 (CLIP-170) regulates microtubule stability and dynein activation. Dev. Cell *6*, 815–829.

Cassimeris, L. (1999). Accessory protein regulation of microtubule dynamics throughout the cell cycle. Curr. Opin. Cell Biol. *11*, 134–141.

CCP4 (Collaborative Computational Project, Number 4)(1994). The CCP4 suit: programs for protein crystallography. Acta Crystallogr. D Biol. Crystallogr. *50*, 760–763.

Delaglio, F., Grzesiek, S., Vuister, G.W., Zhu, G., Pfeifer, J., and Bax, A. (1995). NMRPipe: a multidimensional spectral processing system based on UNIX pipes. J. Biomol. NMR *6*, 277–293.

DeLano, W.L. (2001). The PyMOL Molecular Graphics System (http://www.pymol.org).

Desai, A., and Mitchison, T.J. (1997). Microtubule polymerization dynamics. Annu. Rev. Cell Dev. Biol. *13*, 83–117.

Fodde, R., Kuipers, J., Rosenberg, C., Smits, R., Kielman, M., Gaspar, C., van Es, J.H., Breukel, C., Wiegant, J., Giles, R.H., et al. (2001). Mutations in the APC tumour suppressor gene cause chromosomal instability. Nat. Cell Biol. *3*, 433–438.

Gimona, M., Djinovic-Carugo, K., Kranewitter, W.J., and Winder, S.J. (2002). Functional plasticity of CH domains. FEBS Lett. *513*, 98–106.

Gill, S.R., Schroer, T.A., Szilak, I., Steuer, E.R., Sheetz, M.P., and Cleveland, D.W. (1991). Dynactin, a conserved, ubiquitously expressed component of an activator of vesicle motility mediated by cytoplasmic dynein. J. Cell Biol. *115*, 1639–1650.

Goldsmith, S.C., Pokala, N., Shen, W., Fedoorov, A.A., Matsudaira, P., and Almo, S.C. (1997). The structure of an actin-crosslinking domain from human fimbrin. Nat. Struct. Biol. *4*, 708–712.

Hayashi, I., and Ikura, M. (2003). Crystal structure of the amino-terminal microtubule-binding domain of end-binding protein 1 (EB1). J. Biol. Chem. *278*, 36430–36434.

Honnappa, S., John, C.M., Kostrewa, D., Winkler, F.K., and Steinmetz, M.O. (2005). Structural insights into the EB1–APC interaction. EMBO J. *24*, 261–269.

Hoogenraad, C.C., Akhmanova, A., Grosveld, F., De Zeeuw, C.I., and Galjart, N. (2000). Functional analysis of CLIP-115 and its binding to microtubules. J. Cell Sci. *113*, 2285–2297.

Howard, J., and Hyman, A.A. (2003). Dynamics and mechanics of the microtubule plus end. Nature *422*, 753–758.

Hyman, A., Drechsel, D., Kellogg, D., Salser, S., Sawin, K., Steffen, P., Wordeman, L., and Mitchison, T. (1991). Preparation of modified tubulins. Methods Enzymol. *196*, 478–485.

Keep, N.H., Winder, S.J., Moores, C.A., Walke, S., Norwood, F.L., and Kendrick-Jones, J. (1999). Crystal structure of the actin-binding region of utrophin reveals a head-to-tail dimer. Structure *15*, 1539–1546.

Lansbergen, G., Komarova, Y., Modesti, M., Wyman, C., Hoogenraad, C.C., Goodson, H.V., Lemaitre, R.P., Drechsel, D.N., van Munster, E., Gadella, T.W., et al. (2004). Conformational changes in CLIP-170 regulate its binding to microtubules and dynactin localization. J. Cell Biol. *166*, 1003–1014.

Li, S., Finley, J., Liu, Z.J., Qiu, S.H., Chen, H., Luan, C.H., Carson, M., Tsao, J., Johnson, D., Lin, G., et al. (2002). Crystal structure of the cytoskeleton-associated protein glycine-rich (CAP-Gly) domain. J. Biol. Chem. *277*, 48596–48601.

Ligon, L.A., Shelly, S.S., Tokito, M., and Holzbaur, E.L. (2003). The microtubule plus-end proteins EB1 and dynactin have differential effects on microtubule polymerization. Mol. Biol. Cell *14*, 1405–1417.

Lim, W.A. (2002). The modular logic of signaling proteins: building allosteric switches from simple binding domains. Curr. Opin. Struct. Biol. *12*, 61–68.

Lippincott, J., and Li, R. (1998). Sequential assembly of myosin II, an IQGAP-like protein, and filamentous actin to a ring structure involved in budding yeast cytokinesis. J. Cell Biol. *140*, 355–366.

Mateer, S.C., Morris, L.E., Cromer, D.A., Bensenor, L.B., and Bloom, G.S. (2004). Actin filament binding by a monomeric IQGAP1 fragment with a single calponin homology domain. Cell Motil. Cytoskeleton *58*, 231–241.

McRee, D.E. (1999). XtalView/Xfit–A versatile program for manipulating atomic coordinates and electron density. J. Struct. Biol. *125*, 156–165.

Mimori-Kiyosue, Y., Shiina, N., and Tsukita, S. (2000a). The dynamic behavior of the APC-binding protein EB1 on the distal ends of microtubules. Curr. Biol. *10*, 865–868.

Mimori-Kiyosue, Y., Shiina, N., and Tsukita, S. (2000b). Adenomatous polyposis coli (APC) protein moves along microtubules and concentrates at their growing ends in epithelial cells. J. Cell Biol. *148*, 505–518.

Mimori-Kiyosue, Y., and Tsukita, S. (2003). "Search-and-capture" of microtubules through plus-end-binding proteins (+TIPs). J. Biochem. (Tokyo) *134*, 321–326.

Mitchison, T., and Kirschner, M. (1984). Dynamic instability of microtubule growth. Nature *312*, 237–242.

Morrison, E.E., Wardleworth, B.N., Askham, J.M., Markham, A.F., and Meredith, D.M. (1998). EB1, a protein which interacts with the APC tumour suppressor, is associated with the microtubule cytoskeleton throughout the cell cycle. Oncogene *17*, 3471–3477.

Munemitsu, S., Souza, B., Muller, O., Albert, I., Rubinfeld, B., and Polakis, P. (1994). The APC gene product associates with microtubules in vivo and promotes their assembly in vitro. Cancer Res. *54*, 3676–3681.

Nakamura, M., Zhou, X.Z., and Lu, K.P. (2001). Critical role for the EB1 and APC interaction in the regulation of microtubule polymerization. Curr. Biol. *11*, 1062–1067.

Nogales, E., Wolf, S.G., and Downing, K.H. (1998). Structure of the alpha beta tubulin dimer by electron crystallography. Nature *391*, 199–203.

Otwinowski, Z., and Minor, W. (1997). Processing of X-ray diffraction data collected in oscillation mode. Methods Enzymol. *276*, 307–326.

Perez, F., Diamantopoulos, G.S., Stalder, R., and Kreis, T.E. (1999). CLIP-170 highlights growing microtubule ends in vivo. Cell *96*, 517–527.

Perrakis, A., Morris, R., and Lamzin, V.S. (1999). Automated protein model building combined with iterative structure refinement. Nat. Struct. Biol. *6*, 458–463.

Sattler, M., Schleucher, J., and Griesinger, C. (1999). Heteronuclear multidimensional NMR experiments for the structure determination of proteins in solution employing pulsed field gradients. Prog. NMR Spectrosc *34*, 93–158.

Schiff, P.B., Fant, J., and Horwitz, S.B. (1979). Promotion of microtubule assembly in vitro by taxol. Nature *277*, 665–667.

Schroer, T.A. (2001). Microtubules don and doff their caps: dynamic attachments at plus and minus ends. Curr. Opin. Cell Biol. *13*, 92–96.

Schuyler, S.C., and Pellman, D. (2001). Microtubule "plus-end-tracking proteins": the end is just the beginning. Cell *105*, 421–424.

Slep, K.C., Rogers, S.L., Elliott, S.L., Ohkura, H., Kolodziej, P.A., and Vale, R.D. (2005). Structural determinants for EB1-mediated recruitment of APC and spectraplakins to the microtubule plus end. J. Cell Biol. *168*, 587–598.

Su, L.K., Burrell, M., Hill, D.E., Gyuris, J., Brent, R., Wiltshire, R., Trent, J., Vogelstein, B., and Kinzler, K.W. (1995). APC binds to the novel protein EB1. Cancer Res. *55*, 2972–2977.

Terwilliger, T.C., and Berendzen, J. (1999). Automated MAD and MIR structure solution. Acta Crystallogr. D *50*, 849–861.

Tirnauer, J.S., O'Toole, E., Berrueta, L., Bierer, B.E., and Pellman, D. (1999). Yeast Bim1p promotes the G1-specific dynamics of microtubules. J. Cell Biol. *145*, 993–1007.

Tirnauer, J.S., Canman, J.C., Salmon, E.D., and Mitchison, T.J. (2002a). EB1 targets to kinetochores with attached, polymerizing microtubules. Mol. Biol. Cell *13*, 4308–4316.

Tirnauer, J.S., Grego, S., Salmon, E.D., and Mitchison, T.J. (2002b). EB1-microtubule interactions in Xenopus egg extracts: role of EB1 in microtubule stabilization and mechanisms of targeting to microtubules. Mol. Biol. Cell *13*, 3614–3626.

Vaughan, P.S., Miura, P., Henderson, M., Byrne, B., and Vaughan, K.T. (2002). A role for regulated binding of p150(Glued) to microtubule plus ends in organelle transport. J. Cell Biol. *158*, 305–319.

Waterman-Storer, C.M., Karki, S., and Holzbaur, E.L. (1995). The p150Glued component of the dynactin complex binds to both microtubules and the actin-related protein centractin (Arp-1). Proc. Natl. Acad. Sci. USA *92*, 1634–1638.

Wen, Y., Eng, C.H., Schmoranzer, J., Cabrera-Poch, N., Morris, E.J., Chen, M., Wallar, B.J., Alberts, A.S., and Gundersen, G.G. (2004). EB1 and APC bind to mDia to stabilize microtubules downstream of Rho and promote cell migration. Nat. Cell Biol. *6*, 820–830.

Zumbrunn, J., Kinoshita, K., Hyman, A.A., and Näthke, I.S. (2001). Binding of the adenomatous polyposis coli protein to microtubules increases microtubule stability and is regulated by GSK3 beta phosphorylation. Curr. Biol. *11*, 44–49.

Accession Numbers

The coordinates have been deposited in the Protein Data Bank (accession code 1TXQ).